

Theo yêu cầu của khách hàng, trong một năm qua, chúng tôi đã dịch qua 16 môn học, 34 cuốn sách, 43 bài báo, 5 sổ tay (chưa tính các tài liệu từ năm 2010 trở về trước) Xem ở đây

**DỊCH VỤ  
DỊCH  
TIẾNG  
ANH  
CHUYÊN  
NGÀNH  
NHANH  
NHẤT VÀ  
CHÍNH  
XÁC  
NHẤT**

Chỉ sau một lần liên lạc, việc dịch được tiến hành

Giá cả: có thể giảm đến 10 nghìn/1 trang

Chất lượng: Tao dung niềm tin cho khách hàng bằng công nghệ 1. Bạn thấy được toàn bộ bản dịch; 2. Bạn đánh giá chất lượng. 3. Bạn quyết định thanh toán.

Tài liệu này được dịch sang tiếng Việt bởi:

**[www.mientayvn.com](http://www.mientayvn.com)**

Hướng dẫn truy cập: Ctrl+click vào các link bên dưới

Từ bản gốc:

<https://drive.google.com/folderview?id=0B4rAPqlxIMRDUBEMnZoemFHM00&usp=sharing>

Liên hệ mua:

[thanhlam1910\\_2006@yahoo.com](mailto:thanhlam1910_2006@yahoo.com) hoặc [frbwrthes@gmail.com](mailto:frbwrthes@gmail.com) hoặc số 0168 8557 403

Giá tiền: 1 nghìn/trang đơn (không chia cột); 500 VND/trang song ngữ

Dịch tài liệu của bạn: [http://www.mientayvn.com/dich\\_tiang\\_anh\\_chuyen\\_nghanh.html](http://www.mientayvn.com/dich_tiang_anh_chuyen_nghanh.html)

## CHAPTER 6 THE CALCULATION OF SOLAR EFFICIENCY

One of the goals of the past few chapters has been the calculation of the solar efficiency  $\eta_s$ . The current-voltage J-V characteristics of an ideal cell with a single dominant current transport mechanism can be represented by an expression such as  $J = J_0[\exp(qV/kT) - 1] - J_L$ , (6.1)

at least over the range of J values that determine the solar efficiency. The dark J-V curve is translated downward by the magnitude of the light-generated current  $J_L$  without change in shape, as shown in Fig. 6.1. This, ideal characteristic is the result of superposition and in this case the short-circuit current =  $-J_L$ .

In most cases the following general steps are involved in the calculation of solar efficiency.

1. Calculation of the total light-generated current  $J_L$  from the incident spectral photon flux, the bulk semiconductor parameters [the absorption constant  $a(\lambda)$ , the minority carrier diffusion length  $L_n$ , and the surface recombination velocity  $S$ ], and the geometry of the device.

2. Calculation of the maximum power  $P_m$  using the J-V relationship of the diode and the  $J_L$  value.

Considered in detail, this calculation would also involve grid coverage and reflection losses.

3. Calculation of the solar efficiency  $\eta_s = P_m/P_t$  (6.2)

using the total solar input power  $P_t$

These steps are not always independent, as is discussed toward

## Chương 6 TÍNH HIỆU SUẤT PIN MẶT TRỜI

Trong một số chương trước đây, một trong những mục tiêu của chúng ta là tính toán hiệu suất pin mặt trời  $\eta_s$ . Đối với pin lý tưởng có một cơ chế vận chuyển dòng chiếm ưu thế, đặc tuyến dòng-áp J-V của nó có dạng

$$J = J_0[\exp(qV/kT) - 1] - J_L, \quad (6.1)$$

ít nhất trên một khoảng giá trị J xác định hiệu suất pin mặt trời. Đường cong J-V tối dịch xuống phía dưới một đoạn bằng độ lớn của dòng do ánh sáng tạo ra  $J_L$  và hình dạng không thay đổi, xem hình 6.1. Đặc tuyến lý tưởng này là kết quả của sự chồng chất và trong trường hợp này dòng ngắn mạch  $J_{sc} = -|J_L|$ .

Trong đa số trường hợp, chúng ta tính toán hiệu suất pin mặt trời qua một số bước như sau.

1. Tính dòng toàn phần  $J_L$  do ánh sáng tạo ra từ phổ thông lượng photon tới, các tham số của bán dẫn khối [hằng số hấp thụ  $\alpha(\lambda)$ , chiều dài khuếch tán của hạt tải điện thiểu số  $L_n$ , và vận tốc tái hợp bề mặt  $S$ ], và hình dạng của các thiết bị.

2. Tính toán công suất cực đại  $P_m$  bằng hệ thức J-V của diode và giá trị  $J_L$ .

Nếu xét chi tiết, tính toán này cũng có liên quan đến grid coverage (phủ lưới) và sự tổn hao phản xạ.

3. Tính hiệu suất pin mặt trời

$$\eta_s = P_m/P_t \quad (6.2)$$

bằng công suất đầu vào toàn phần của ánh sáng mặt trời  $P_t$ . Khi tiến dần đến cuối chương, chúng ta sẽ thấy những bước này không hoàn toàn độc lập.

the end of this chapter.

Two additional quantities are important. The open-circuit voltage is given by

$$= (kT/q) \ln[(J_L/J_0) + 1],$$

The fill factor ff, given by

$$P_m/J_{sc}V_{oc}, \quad (6.3)$$

is a measure of the “squareness” of the J-V curve. In terms of  $V_{oc}$  and ff the solar efficiency is given by

$$\eta_s = V_{oc} |J_{sc}| ff / P_s.$$

Although the fundamental parameters of the solar cell are  $J_L$ ,  $J_0$ ,  $A$ , and  $R_s$ , the usual description is in terms of  $V_{oc}$  and ff. These parameters are useful, intuitive, and easily measured. For nearly ideal cells  $J_{sc}$ ,  $V_{oc}$ , and ff have been usually treated almost as independent parameters in the literature. This independence is even more of an approximation for less-than-ideal cells, such as those under high-intensity illumination or those with transport dominated by interface recombination. Properly, the nonideal cells must be treated as a whole. There are three methods of attacking the solar efficiency problem.

1. By superposition, assuming that the light and dark currents are linearly additive, an exact solution can be obtained for the ideal cell, including the presence of simple, lumped values of series and parallel resistance.

2. The nonideal cell can be treated by analysis in terms of perturbations on the ideal cell parameters.

3. By the computer-numerical solution of the transport equation simultaneously with the other

$$V_{oc} = (kT/q) \ln[(J_L/J_0) + 1].$$

$$ff \equiv P_m / J_{sc} V_{oc}, \quad (6.3)$$

$$\eta_s = V_{oc} |J_{sc}| ff / P_s.$$

relevant equations, nonideal and three di-mensional cells may be treated by a holistic approach.

The implications of superposition are discussed by Lindholm et al. (1976, 1979) for a general case, by Rothwarf (1978) for the CutS/CdS cell, and by Tarr and Pulfrey (1979) for Si and GaAs cells at  $C = 1$ .

In the first section of this chapter, we discuss the calculation of  $TJ^*$  for VOLTAGE (V)

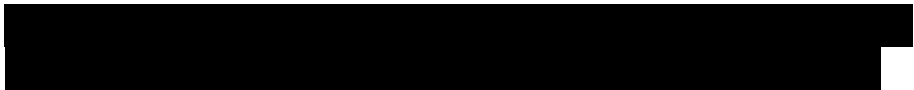
Fig. 6.1. Light and dark J- V curves for an ideal cell. The power output is shown by the dashed curve.

an ideal cell and derive the relation of  $t_{js}$  to  $J_0$  and  $A$ . Next we discuss the dependence of on series and parallel resistance ( $R^*$  and  $R_0$ ) and, finally, we consider four related topics: the calculation of solar efficiency by perturbation analysis (Section 6.3.1) and by global computer numerical solution, the dependence of  $J_0$  and  $A$  on illumination, the variation of  $t_{jb}$  with temperature and illumination level, and, finally, an energy loss analysis.

### 6.1 THE IDEAL CELL UNDER ILLUMINATION < >

In this section we calculate the solar efficiency of an ideal cell in which the law of superposition holds. The implications of this model are as follows.

1. For a range of illumination intensities below and including that for intended use,  $J_a$  and the slope of the log J versus V curve are not functions of illumination intensity or wavelength, and so the log  $J$ , versus



Voc curve is identical with the dark log J versus V curve.

2.  $J_L$  is not a function of bias voltage.

Fig. 6.2. Solar photon flux distribution  $dV/dE$  at AM1.5 versus photon energy. The dashed curve is the derivative of the polynomial approximation of Fig. 6.3. [Drawn from data in "Terrestrial Photovoltaic Measurement Procedures." NASA (prepared for ERDA), ERDA/NASA/1022.77/16. NASA TM 73702 (1977).]

3.  $R_s \rightarrow 0$  and  $R_p \rightarrow 0$ , i.e., there are no resistance losses.

The total light-generated current is given by the integration of the product of  $TQ(K)$  [or  $tq(E)$ ] and the solar photon flux  $dV/d\lambda$  (or  $dT/dE$ ):

$$J_L = q \int_0^\infty TQ(E) (dT/dE) dE \quad (6.4)$$

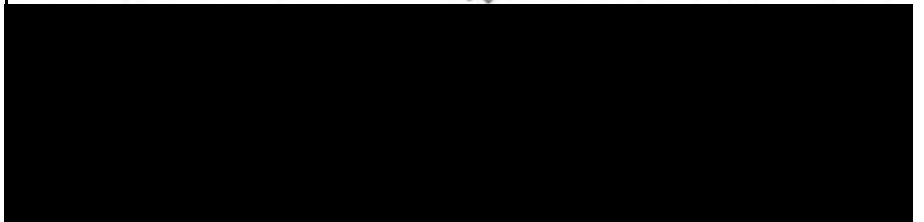
Note that the quantum efficiency may be a function of intensity as well. The AM 1.5 solar photon flux is shown in Fig. 6.2. The integral of the solar photon flux, shown in Figs. 6.3 and 6.4, is useful for estimation purposes; if we assume  $TQ = 1$ , then  $J_L = q \int_0^\infty (dT/dE) dE = -J_{sc}$ .

The power produced by the cell is  $P = J(V)V$  as indicated in Fig. 6.1 and the maximum power point  $P_m$  is found by maximization of  $J(V)V$ . The value of  $P_m$  (or equivalently  $ff$ ) cannot be obtained explicitly. However, by iteration  $P_m$  can be obtained to any desired accuracy; such a scheme is described here.

These data are tabulated in Appendix 1.



$$J_L = q \int_0^\infty \eta_Q(\lambda) (d\Gamma/d\lambda) d\lambda = q \int_0^\infty \eta_Q(E) (dT/dE) dE \quad (6.4)$$



$$J_L \approx q \int_0^\infty (dT/dE) dE \approx -J_{sc}$$



◆ This treatment has been expanded to include  $R_{sc}$ ,  $R_{sh}$ , and a bias-voltage-dependent quantum efficiency  $\eta$  by Mitchell et al. (1976).

Fig. 6.3. AM 1.5 solar photon flux distribution integrated with respect to photon energy versus lower integration limit (HE)  $-(t/T/dE) dE$  versus  $E = Ac/A$ . Total irradiance  $P_t = 83.2 \text{ mW cm}^{-2}$ . Curve may be fitted approximately for  $E > 0.9 \text{ eV}$  by  $R(E) = A(B - E)^n$ , where  $A = 2.99 \times 10^{11} \text{ photons cm}^{-1} \text{ sec}^{-1} \text{ eV}^{-1}$ ,  $B = 3.485 \text{ eV}$ , and  $n = 2.35$ . [Data from "Terrestrial Photovoltaic Measurement Procedures," NASA (prepared for KRDA) ERDA/NASA/1022-77/16, NASA TM 73702 (1977).]

Since the active, light-absorbing area of the cell  $A$  is likely to be slightly smaller than the total area seen by the diode  $A_D$ , it is convenient to work in terms of currents:

(6.5)

At the maximum power point  $P_m = V_m I_m$  the derivative  $dP/dV = 0$ .

A parameter  $\beta$  is defined as

$$\beta = (I_L + I_m)/I_L, \quad (6.6)$$

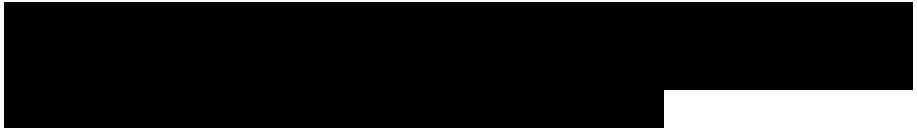
where  $I_i = I_L + I_m$ ,  $I_m < 0$ . This is the ratio of the current passing in the forward direction through the diode biased at  $V_m$  in the dark to  $I_L$ . By convention,  $I_L > 0$  and  $I_m < 0$ . From the equation obtained by setting  $dP/dV = 0$  for Eq. (6.1) it can be shown that

$$0 = V_m/I_L \exp(qV_m/AkT) = 1 / [(qV_m/AkT) + 1]. \quad (6.7)$$

Equation (6.7) can be rearranged to eliminate  $(qV_m/AkT)$  and obtain

$$\beta = [1 + \ln(I_m/I_0)]^{-1}. \quad (6.8)$$

Only a few iterations are required to



$$I_L = J_L A_A, \quad I_0 = J_0 A_D.$$



$$\beta = (I_L + I_m)/I_L, \quad (6.6)$$



$$\beta = (I_0/I_L) \exp(qV_m/AkT) = 1 / [(qV_m/AkT) + 1]. \quad (6.7)$$



$$\beta = [1 + \ln(\beta I_L/I_0)]^{-1}. \quad (6.8)$$



obtain (i to four significant figures. For good cells,  $\beta$  is a slowly varying constant such that  $0.04 < \beta < 0.10$ .

The maximum power is given directly in terms of  $\beta$

$$P_m = -I_L(AkT/q) \left( 1 - \beta \right) \ln(\beta I_L/I_0) \quad (6.9)$$

and the fill factor can be obtained by dividing by  $V_{oc} I_{sc}$  (since for  $R_f = 0$ ,  $V_{oc} = I_L/A$ ):

$$ff = P_m / V_{oc} I_{sc} = (1 - \beta) \ln(\beta I_L/I_0) / \ln(I_L/I_0) \quad (6.10)$$

From this result, it is clear that, for an ideal cell without resistance losses, the fill factor is not a function of the diode factor; the diode factor  $A$  is just a scaling factor for the voltage. On the other hand,  $P_m$  and hence  $t_j$ ,

Series or parallel resistance does introduce a small  $A$  dependence on  $ff$ . The extent of this dependence for nonzero values of  $R$ , is shown by Pulfrey (1978), Ghosh et al. (1980) give an alternative approximate expression for  $ff$  for  $R_s \sim 0$ :

Fig. 6.6. Solar conversion efficiency  $\eta$ , versus  $I_L/A$ ,  $I_0$ , and  $A$  for an ideal cell with  $R_s = 0$ . Temperature is  $300\text{K}$  and the incident solar power density is  $P_0 = 100\text{ mW per unit sun}$  (i.e., for a concentration ratio  $C = 1$ ). The running parameter is  $I_L/A$ , where  $A$  is the diode factor. [Redrawn from K. W. Mitchell, Solar Energy Research Institute, private communication (1979).]

are directly proportional to  $A$ . The  $t_j$  for such an ideal diode is shown in Fig. 6.5. The relationship of the photovoltaic parameters is shown in a more general way in Fig. 6.6, where a solar concentration ratio can

$$P_m = -I_L(AkT/q)(1 - \beta) \ln(\beta I_L/I_0) = -I_L(AkT/q)(1 - \beta)^2/\beta, \quad (6.9)$$

$$ff = P_m / V_{oc} I_{sc} = (1 - \beta) \ln(\beta I_L/I_0) / \ln(I_L/I_0). \quad (6.10)$$

$$ff = \left\{ 1 - \frac{1}{\ln(I_{sc}/I_0)} \right\} \left\{ 1 - \frac{\ln[\ln(I_{sc}/I_0)]}{\ln(I_{sc}/I_0)} \right\}$$

also be accounted for.

From these results, it might seem that the best way to increase would be to raise  $A$  or decrease  $J_0$ . However, Fig. 5.29 shows that  $J_0$  increases almost exponentially with increasing  $A$ . Two constant  $r_{js}$  curves, calculated using Eq. (6.9) and shown in Fig. 5.29, demonstrate this relationship and show that maximizing  $T)S$  is more subtle than merely decreasing  $J_0$  or increasing  $A$ .

No treatment of photovoltaics is complete without at least some comment on maximum theoretical efficiency. The relation between theoretical efficiency and semiconductor band gap for p-n junction cells was established early by a number of researchers including Prince (1955), Loferski (1956), Wolf (1960), and others, using rather ideal material properties and

Fig. 6.7. Theoretical solar efficiency versus semiconductor band gap for ideal homojunction cells ( $A \cdot I$ ) with no surface recombination losses. The variation with temperature is also shown. For AMO solar input. [Figure from S. M. Sze. "Physics of Semiconductor Devices," p. 644, Wiley, New York (1969) (redrawn by Sze after J. J. Wysocki and P. Rappaport, J. Appl. Phys. 31, 571 (1960).]

idealized junction models. Although the magnitudes of the predicted % are quite dependent on the parameters chosen, the maxima of the curves lie close to 1.4-1.5 eV (Fig. 6.7).

For higher temperatures the maximum move to higher band gaps. The efficiency curves represent the compromise between the number of solar photons usefully absorbed by the cell (which decreases as  $E_t$  increases) and the thermally activated forward-bias diode current (which decreases as  $E_g$  increases, thereby increasing  $V_{oc}$ ).

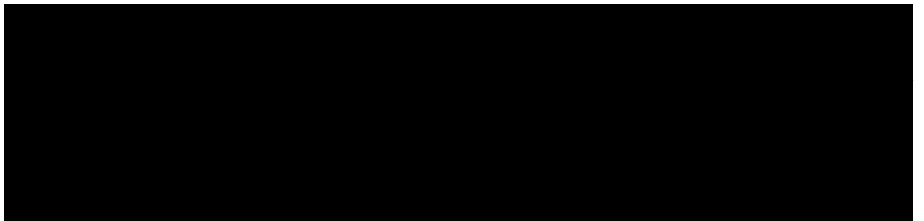
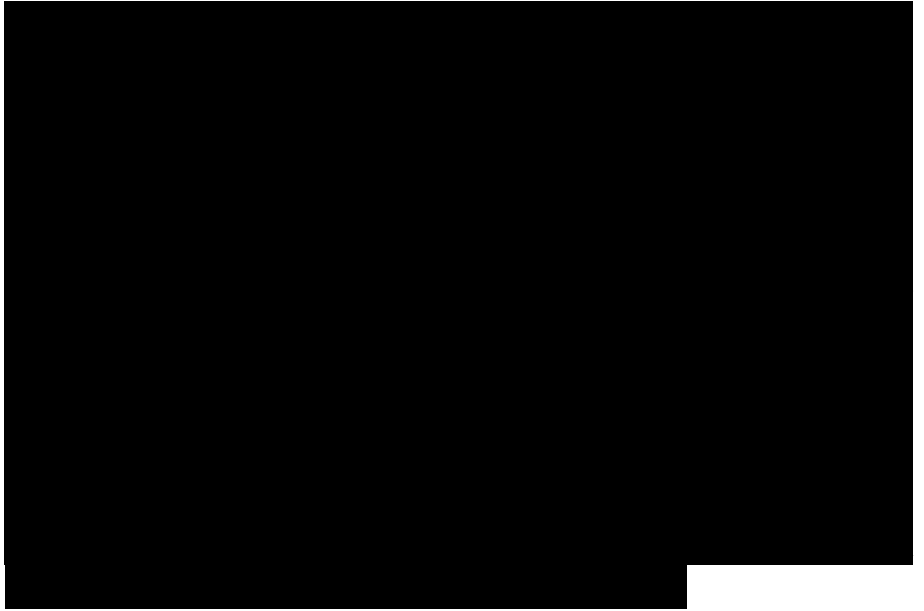
Wolf (1971) shows a set of theoretical efficiency calculations for the Si cell for various assumptions about the materials and device properties. For example, he obtains  $\eta = 22\%$  and  $V_{oc} = 0.788$  at AMO (for  $\tau_n = 10$  ptsec and  $J_0 = 2.4 \times 10^{-15}$  A cm<sup>-2</sup>). The effects of variation of minority carrier lifetime on  $\eta$ ,  $ff$ ,  $V_{oc}$ , and  $J_0$  are given by Graff and Fischer (1979) for Si-based cells.

Theoretical efficiency predictions for heterojunction solar cells are difficult to make because of lack of knowledge about junction transport. In many heterojunctions the dominant mechanism is recombination in the depletion layer, but the transport may be modified so much by interfacial recombination, band-edge discontinuities, and tunneling that  $J_0$  and  $A$  cannot be predicted. However, if we naively assume that junction transport is dominated by injection and diffusion in the absorber quasineutral region ( $A = 1$ ), then the theoretical solar efficiency curves shown in Fig. 6.8 can be readily calculated. No useful absorption in the window layer and reasonably high values of  $r$  and  $n$  have been assumed. These considerations again

favor an absorber band gap of about 1.4 eV, since both absorption and the principal diode current are determined by the absorber in this example. More elaborate predictions for heterojunction solar efficiency have been made by Sreedhar et al. (1969) and Sahai and Milnes (1970). Since the predicted efficiencies are so dependent on material and device properties, it is of interest to determine a maximum theoretical efficiency based on broader principles. This was done by Shockley and Queisser (1961) on the basis of detailed balance of blackbody radiation fluxes between the sun and the solar cell and the assumption, "that each photon (entering the cell) with  $h\nu > E_g$ , produces one electronic charge  $q$  at a voltage of  $V \ll E_g/q$ ." For the further assumptions of unit solar concentration ratio and that the only mode of recombination in the semiconductor was radiative and band-to-band, they found a detailed balance limit of 30% for an optimal band-gap energy of 1.1 eV. This is curiously close to the band-gap energy of Si—the most abundant solid element.

The discussion section of this paper points out several of the problems facing photovoltaic science (such as discrepancies between observed and predicted  $A$  factors,  $J_{sc}$  values, and  $V_{oc}$  values) that are still unresolved.

Fig. 6.8. Naive calculation of maximum theoretical solar efficiency for ideal heterojunction solar cells ( $A - I$ ) versus window layer band-gap energy  $E_g$ , for various



absorber layer band gaps  $E_g$ .  
 Assumptions:  $\tau = 1$ . total area usage, AM1.5 spectrum from Fig. 6.3,  $N_A = 10^{17}$  cm<sup>-3</sup>, all absorber layers are p-type, and the effect of conduction-band discontinuities is neglected.

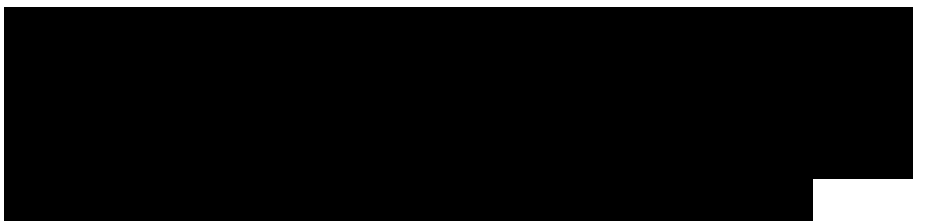
Several other authors have discussed the problem of ultimate efficiency, including Mathers (1977), Landsberg (1977), and De Vos (1980). De Vos, using arguments similar to those of Shockley and Queisser, found a detailed balance limit of  $\eta_j = 40\%$  for a single cell under the theoretical maximum solar concentration ratio  $C = 4.6 \times 10^4$  (see Section 12.1.1). For an infinite number of stacked, tandem cells (Section 12.2.4), they found a limit of  $\eta_{\infty} = 68\%$  for  $C = 1$  and  $\eta^* = 87\%$  for  $C = 4.6 \times 10^4$ .

Using Carnot efficiency arguments. Rose (1960) found an ultimate limit for the open-circuit voltage of  $V_{oc} = (E_g/q)[1 - (T_c/T_r)]$ , where the cell temperature is  $T_c$  and the temperature of the blackbody radiator illuminating the cell is  $T_r$ . This gives  $V_{oc}^* = 1.07$  V for Si. The implicit assumption

Fig. 6.9. Simplified equivalent circuit for a solar cell.

is that the cell-radiator system is reversible, that no photons are lost from the cell-radiator system (implying maximum concentration), and that the exchange is nearly monochromatic with  $E_g < h\nu < E_g + kT_c$ . The results of Shockley and Queisser (1961) indicate an ultimate  $V_{oc} =$

0.83 V (they used  $E_g = 1.09$  eV for Si; if this is adjusted to  $E_g = 1.11$  eV,  $V_{oc} = 0.85$  V).



## 6.2 THE EFFECTS OF SERIES AND PARALLEL RESISTANCE

In any real cell  $R_s > 0$  and  $R_v < \ll$ , resulting in some power losses. In this section the contributions to  $R_s$  and  $R_v$ , are discussed and means to evaluate their effects are considered. In many devices, it is sufficient to lump  $R_s$  and  $R_v$  contributions into the equivalent circuit shown in Fig. 6.9,1. e., a current source shunted by a diode and  $R_p$ , all in series with  $R_s$ , to produce a terminal voltage  $V$  and current  $I$ . To obtain more precise evaluation, particularly in the case of thin, resistive films in the current path, various distributed resistance models must be used that may be evaluated by numerical or analytic means. Finally, the physical origins of  $R_s$ ,  $R_p$ , and the contact resistance are briefly considered.

### 6.2.1 First-Order Evaluation of $R_s$ and $R_v$ Losses

The effect of simple  $R_s$  on a cell can be illustrated by the graphical addition, at constant current, of the I-V characteristic of the cell and a resistance characteristic with slope  $\sqrt{R_s}$  in Fig. 6.10. It is seen that  $V_{oc}$  is unchanged by simple  $R_s$ , and that  $I_{sc}$  is changed very little unless  $R_s$  is quite large, in which case the cell characteristic approaches  $\sqrt{R_t}$  and  $\eta$  approaches 0.25. Similarly, the characteristic for simple  $R_v$  can be obtained by addition, at constant voltage, of the zero resistance I-V curve and  $1/R_v$ . It is seen in this case that  $I_{sc}$  is unchanged whereas  $V_{oc}$  may be changed slightly.'

An approximate limit on  $R_s$  for small power loss can be obtained by Fig. 6.10. The effects of series and

parallel resistance on the I-V characteristics of an ideal solar cell by graphical construction

assuming that the cell operates near the maximum power point and all the loss can be attributed to  $J_s R_s$ . Then the power loss fraction is given by

$$X_s = \frac{J_m^2 R_s}{J_m V_m} = \frac{J_m R_s}{V_m} = \frac{J_{sc} R_s}{V_{oc}} \quad (6.11)$$

For a 3% loss at  $J_{sc} = 40 \text{ mA cm}^{-2}$  and  $V_m = 0.6 \text{ V}$ ,  $R_s$  must be less than  $0.5 \text{ } \Omega$  for each square centimeter of cell area.

Similarly, the power loss fraction due to  $R_p$  is given by

$$X_p = \frac{V_m^2 / R_p}{J_m V_m} = \frac{V_m}{J_m R_p} = \frac{V_{oc}}{J_{sc} R_p} \quad (6.12)$$

and for a 3% loss due to  $R_p$ ,  $R_p$  must be greater than  $500 \text{ } \Omega$  for each square centimeter of cell area. These approximations are quite accurate for  $J_{sc} R_s < 5\%$ . For the small-loss case  $V_m$  and  $J_m$  remain almost unchanged and the major effect is the reduction of  $ff$ , approximately by the factor  $(1 - J_{sc} R_s / V_{oc} - V_{oc} / J_{sc} R_p)$ .

The cell characteristic including  $R_s$  and  $R_p$  is given by

$$I = I_0 \{ \exp[q(V - IR_s) / AkT] - 1 \} + (V - IR_s) / R_p - I_L \quad (6.13)$$

With the addition of  $I_L$ ,  $I_L > 0$ , superposition no longer holds and the light J-V curve cannot be described by a simple translation of the dark curve.

The (3) formulation approach of Section 6.1 can be used to obtain accurate  $J_m$  and  $V_m$  values for the simple lumped element circuit of Fig. 6.9. For the case involving only  $R_s$ ,  $t$

$\beta = [1 + \frac{1}{1 + 2R_s I_m \beta(q/AkT)} \ln(\beta I_m / I_0)]^{-1}$  with  $P_m$  given by

[REDACTED]

[REDACTED]

$$X_s = \frac{J_m^2 R_s}{J_m V_m} = \frac{J_m R_s}{V_m} = \frac{J_{sc} R_s}{V_{oc}} \quad (6.11)$$

[REDACTED]

[REDACTED]

$$X_p = \frac{(V_m^2 / R_p) / J_m V_m}{J_m V_m} = \frac{V_m}{J_m R_p} = \frac{V_{oc}}{J_{sc} R_p} \quad (6.12)$$

[REDACTED]

$$(1 - J_{sc} R_s / V_{oc} - V_{oc} / J_{sc} R_p)$$

[REDACTED]

$$I = I_0 \{ \exp[q(V - IR_s) / AkT] - 1 \} + (V - IR_s) / R_p - I_L \quad (6.13)$$

[REDACTED]

[REDACTED]

$$\beta = \left[ 1 + \frac{1}{1 + 2R_s I_m \beta(q/AkT)} \ln(\beta I_m / I_0) \right]^{-1} \quad (6.14)$$

$$P_m = -(AkT/q)H(\beta - p) \ln(I_L/I_0) + R_s I_L^2 (1 - \beta)^2 \quad (6.15)$$

and  $ff$  by

$$ff = P_m / [I_{sc} (AkT/q) \ln(I_L/I_0)] \quad (6.16)$$

The term  $IK$  must remain in the denominator of Eq. (6.16) since for large  $R_s$ ,  $\beta$  may be different from  $\beta^*$ . (which may be quickly found by iteration).

The variation of  $ff$  with  $JL$  (or, equivalently, the light intensity), shown in Fig. 6.11 with the effects of series and parallel resistance, provides a valuable diagnostic tool for preliminary investigation of experimental cells.

### 6.2.2 Distributed Resistance Models

Most solar cells contain a thin front layer in which current is collected laterally by a grid structure. The resistance loss is distributed within the film and more accurate models must be used. An example of such a gridded cell structure is shown in Fig. 6.12. The series resistance of the device includes the following contributions:

$R_Q$  Resistance of the front grid structure

$R_{cl}$ ,  $R_{ct}$  Contact resistances (inversely proportional to contact area)

Equation (6.6) still holds, but Eq. (6.7) is not applicable here.

Fig. 6.12. Current flow paths in a gridded cell structure with the thickness of the front layer  $l$ , much less than that of the base  $t$ .

$R_t(x) = \rho l / wt$  Lateral resistance to current flow along the plane of the film depending on the distance  $x$  (where  $\rho$ , is the bulk resistivity of the film and  $l$  is its thickness)

$$P_m = -(AkT/q)I_L(1 - \beta) \ln(\beta I_L/I_0) + R_s I_L^2 (1 - \beta)^2 \quad (6.15)$$

$$ff = P_m / [I_{sc} (AkT/q) \ln(I_L/I_0)] \quad (6.16)$$

[Redacted]

[Redacted]

[Redacted]

[Redacted]

[Redacted]

[Redacted]

[Redacted]

$R_t$  - Transverse resistance through the base layer (of bulk resistivity  $\rho^*$ , thickness  $t$ , and area  $s d_0$ )

$R_{iZ}$  Spreading resistance of the back contact sheet.

Given the total allowed  $R_{\Sigma}$ , the cell designer can then allocate the contributions according to the material constraints of the device. The application of these ideas to the design of grid structures is discussed by Riemer (1978) and Surreze (1978).

The problem of distributed resistance may be handled approximately by various lumped element equivalent circuits, by analytic solutions using simplifying assumptions, or, more exactly, by computer-numerical solutions for finite element models. Wolf and Rauschenbach (1963) examined models in which  $\rho^*$ s and  $R_{\Sigma}$ , were lumped into second- and higher-order versions of the equivalent circuit shown in Fig. 6.9. Fang and Hauser (1978) and Heizer and Chu (1976) discuss solutions for two-dimensional structures, and Spadema and Navon (1978) give results for three-dimensional structures at high concentration ratios.

The analytic approach can yield useful results for some simple geometries such as the one-dimensional example that follows. Current flow in the front layer is assumed to be in the plane of the layer as shown in Fig. 6.13 whereas the current flow in the base and at the junction is perpendicular to the cell area. Consider an elemental volume of the front layer

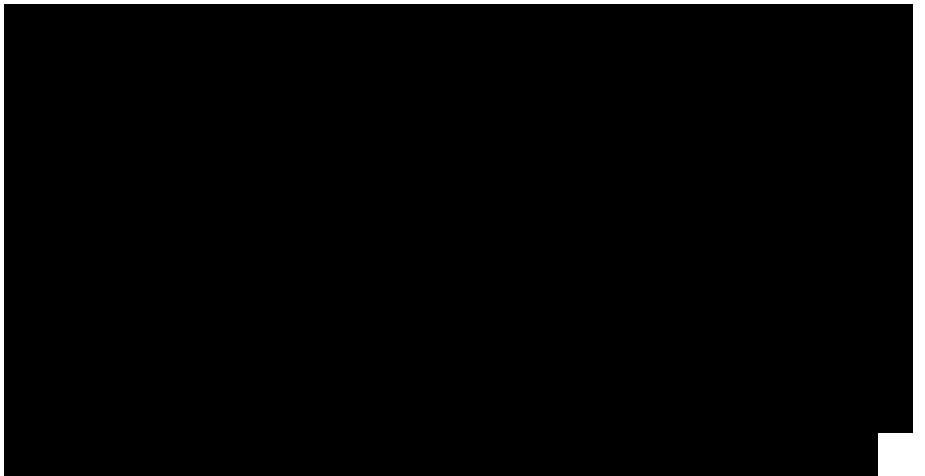


Fig. 6.13. Cross section of front gridded solar cell for analytical distributed resistance analysis.

A junction is bounded by  $x$  and  $x + \Delta x$ . The lateral current density at the two boundaries is  $J_{in} = \rho \frac{dV}{dx}$  and  $J_{out} = \rho \frac{dV}{dx}|_{x+\Delta x}$ . The difference  $J_{out} - J_{in}$  is balanced by the current flow through the junction plane  $J(V)$  at the bias voltage considered:

$$J_{out} - J_{in} = J(V) \Delta x / \rho$$

The quantity  $\frac{dV}{dx}$  can be expanded in a Taylor series about  $x$  to obtain

$$\frac{dV}{dx} \Big|_{x+\Delta x} = \frac{dV}{dx} \Big|_x + \Delta x \frac{d^2V}{dx^2} \Big|_x \quad (6.17)$$

A solution of Eq. (6.17) can be obtained easily by assuming that  $J(V) = J_m$  is a constant (the current at the maximum power point) giving a parabolic relation for  $V(x)$ , shown in Fig. 6.14. If the resistance loss is not too great, the approximation is quite good. The distributed resistance power loss per unit area may be obtained directly in terms of the grid spacing  $\Delta x$ :

$$P_{loss} = J_m^2 \rho \Delta x^3 / 12t_1 \quad (6.18)$$

(or an "equivalent" series resistance of  $R_s = \rho \Delta x / 2t_1$ ). Such analytic results have been obtained by Handy (1975) and Wyeth (1977) for two-dimensional geometries.

By using finite element models for the treatment of the distributed re-

■ A solution for Eq. (6.17) for the case of  $J = J(V)$  is given by Wysocki (1961).

Fig. 6.14. (a) Voltage distribution between grid lines of the cell of Fig. 6.13, for operation near and (b) corresponding voltage values on J- V curve.

sistance problem, accurate results

$$J_{out} \Delta x w - J_{in} \Delta x w = J(V) \Delta x w$$

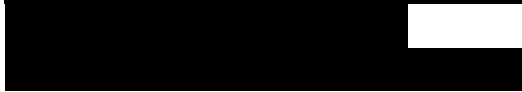
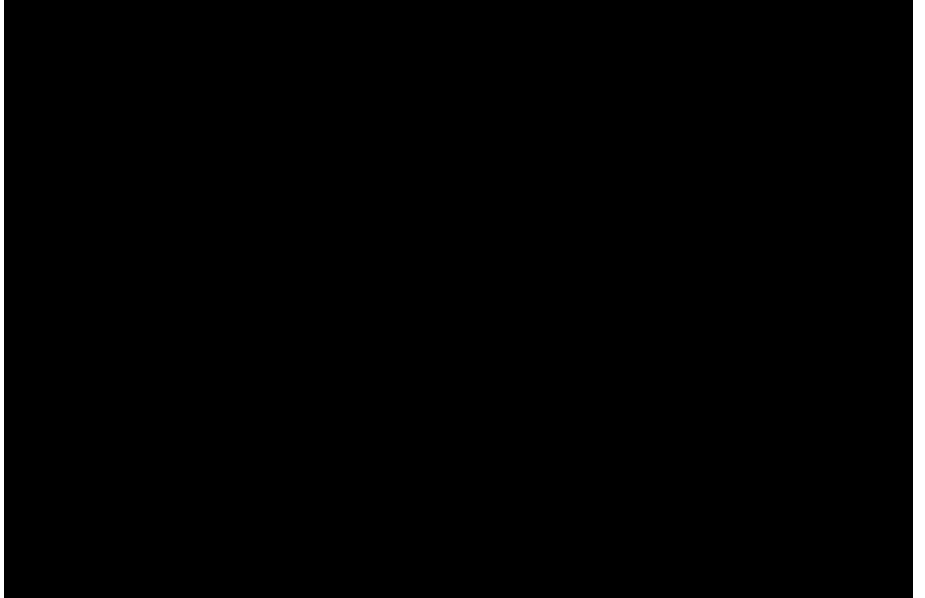
$$\frac{d^2V}{dx^2} = J(V) \rho / t_1 \quad (6.17)$$

$$P_{loss} = J_m^2 \rho \Delta x^3 / 12t_1 \quad (6.18)$$

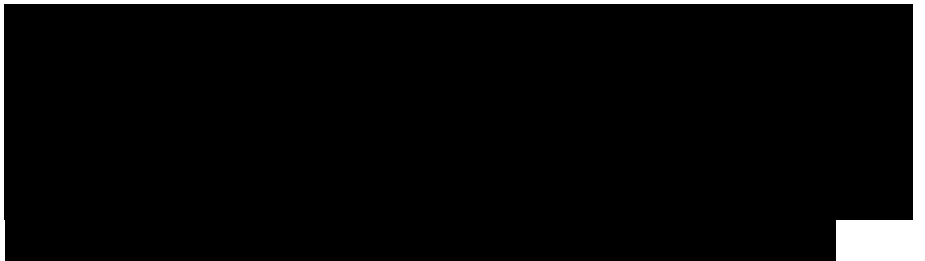
can be obtained for more complex diode relations and geometries, and for both distributed series and parallel resistances. The essence of this method is shown in Fig. 6.15, where the cell is first transformed into a long, half-grid-spacing-wide section, which is then divided into finite elements of width  $\Delta x$ . Since  $x_g/2$  is a symmetry point, no current flows to the right side of the element labeled zero. By assuming a trial voltage  $V(0)$  for this element, the current through the element  $I(0)$ , can easily be calculated, and then  $V(1)$  and the succeeding values up to the terminals of the cell. By varying the trial parameter  $V(0)$ , the terminal I-V curve for the device can be generated for even the most complex diode characteristic. The model is readily extended to two dimensions as has been done by Mitchell (1977). Calculations are done here for a hypothetical heterojunction cell with the following parameters:

$x_g = 0.10 \text{ cm}$        $J_0 = 10^{-9} \text{ A cm}^{-2}$   
 $\mu_D = 1 \text{ cm}^2 \text{ V}^{-1} \text{ s}^{-1}$        $A = 2$   
 $w = 1 \text{ cm}$        $J_L = 0.03 \text{ A cm}^{-2}$   
 $R_s = 0.1 \text{ } \Omega \text{ cm}$   
 $R_{sh} = 2 \times 10^{-4} \text{ } \Omega \text{ cm}^2$  grid coverage = 5%.  
 These calculations indicate a limiting bulk resistivity of about  $0.2 \text{ } \Omega \text{ cm}$  for a negligible power loss in the front layer, as shown in Fig. 6.16.

A result of this analysis is that  $V_{oc}$  can be reduced from its  $R_s = 0$  value by appreciable distributed series resistance because of shunting by the portion of the cell diode structure that is shadowed by the grid. This is especially important for experimental cells when  $R_s^*$  may be quite large, and the grid shadowing



$x_g = 0.10 \text{ cm}$	$J_0 = 10^{-9} \text{ A cm}^{-2}$
$\mu_D = 1 \text{ cm}^2 \text{ V}^{-1} \text{ s}^{-1}$	$A = 2$
$w = 1 \text{ cm}$	$J_L = 0.03 \text{ A cm}^{-2}$



area can be a large fraction of the active area of the cell.

Fig. 6.15. One-dimensional, finite element, distributed parameter model.

### 6.2.3 Physical Origins of Series and Parallel Resistances

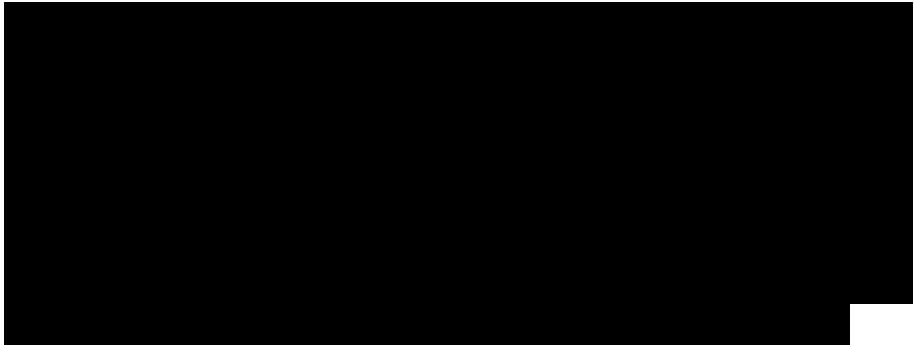
In this section we briefly comment on the physical basis for the contributions to series and parallel resistance listed in Section 6.2.2.

The bulk resistivity contributions of the emitter and base regions to  $R_s$  are quite different because of the geometrical factors involved. Thus, for negligible loss in the thin front layers, where current flow is along the layer, resistivities of  $p < 0.001$ - $1 \text{ } \Omega\text{-cm}$  are required, whereas for the heterojunction  $p < 25$ - $1000 \text{ } \Omega\text{-cm}$  is sufficient. The thin front layers of heterojunction cells are polycrystalline in some cases so that the mobility is limited by grain-boundary barriers and the resistivity may be highly anisotropic. In these cases either very high carrier densities are required or a transparent conducting window layer must be applied. This is discussed in more detail in Chapter 9.

Fig. 6.16. Calculated solar efficiency versus window layer resistivity. Cell parameters given in text. Efficiency for total  $R_s = 0$  is also shown. Inset shows voltage distribution between two grid lines for  $1 \text{ } \Omega\text{-cm}$  resistivity when cell is operating at the maximum power point.

The bulk contribution from

The bulk contribution from



insulating layers within the cell (such as depletion layers or the insulating layer in a p/i/n structure) is more complex. If the layer is thinner than the carrier diffusion length as modified by the local electric field (Section 4.5.1), then the resistance is essentially zero. For layers much thicker than  $L \gg L^*$  and/or  $L \gg L^*$ , the current transport is modified by space-charge-limited flow and, for high injected currents, a  $J \propto V^{3/2}$  dependence occurs rather than an ohmic resistance. These cases are discussed by Rose (1964).

For high solar concentration ratios, the photogenerated carrier density can modulate the conductivity as both minority and majority carrier density are increased by photogeneration ( $n \rightarrow p$ ). Under these conditions the larger the current generated, the greater the majority carrier density; the voltage drop across the cell may be limited to a few  $kT$ , independent of  $A-N$

(if the grid lines on the front layer of a cell can be spaced less than a majority carrier diffusion length apart, then the transport is controlled by diffusion rather than drift and the voltage drop between grid lines is of the order of only  $kT$ ).

The contact resistance  $R_c$  is perhaps the most overlooked (and frustrating) contribution to  $R_s$  in experimental cells. Indeed many "ohmic" contacts are, in reality, leaky Schottky diodes with nonlinear characteristics. Figure 6.17 shows the contribution of such a "quasi-ohmic" contact to the dark and light cell characteristics. In this case the "forward" characteristic of the contact is operative in the



illuminated, power-generating mode. The theory of ohmic contacts is outlined in Section 5.8.

Fig. 6.17. The effect of a nonohmic contact on the J- V characteristics of a solar cell. The dashed lines are the J- V characteristic of the nonohmic contact alone and the resulting cell terminal characteristics.

Contact resistance can be measured by various schemes as discussed by Berger, (1972) and Cox and Strack (1967). The essence of one of these measurements is illustrated by the three-point technique shown in Fig. 6.18. Contact 3, connected to a high-impedance voltmeter, draws negligible current and thus the voltage drop across this contact is also negligible; contact 3 senses the potential just inside the semiconductor. Variation of the current through contacts 2 (and 2') and 1 yields the I-V characteristic of contacts 2 and 2' and the contact resistance  $R_c$ . Such data must be interpreted with care since some contacting operations can leave a skin of highly conducting material on the surface of the semiconductor that essentially shorts contacts 2 and 3 and gives exaggeratedly small values of  $R_c$ . The specific contact resistivity is defined by

$\rho_{c0} = dV/dJ \cdot A_c = (\Omega \text{ cm}^2)$ ,  
 where  $A_c$  is the contact area. Most contacts are only semi-ohmic so that  $\rho_c = \rho_c(V)$ . Since we are interested in the solar cell contact voltage drop  $\Delta V$  during operation, it is convenient to use an effective contact resistivity given by  
 $\rho_c = \Delta V/J^*$ ,



$$\rho_{c0} = dV/dJ|_{V=0} = R_{c0} \cdot A_c \quad (\Omega \text{ cm}^2), \quad (6.19)$$



$$\rho_c = \Delta V/J_m,$$

where  $J_m$  is the current density at the maximum power point for the desired solar concentration ratio, as shown in Fig. 6.18.

Fig. 6.18. (a) Three-point measurement of contact resistivity (of contacts 2 and 2') with (b) resulting J- V curve. As a working value for  $r_c$ , it is convenient to give the reciprocal of the slope of the line through the J-V value at  $J \cdot J_n(\text{AMI})$  for a cell operating at AMI.

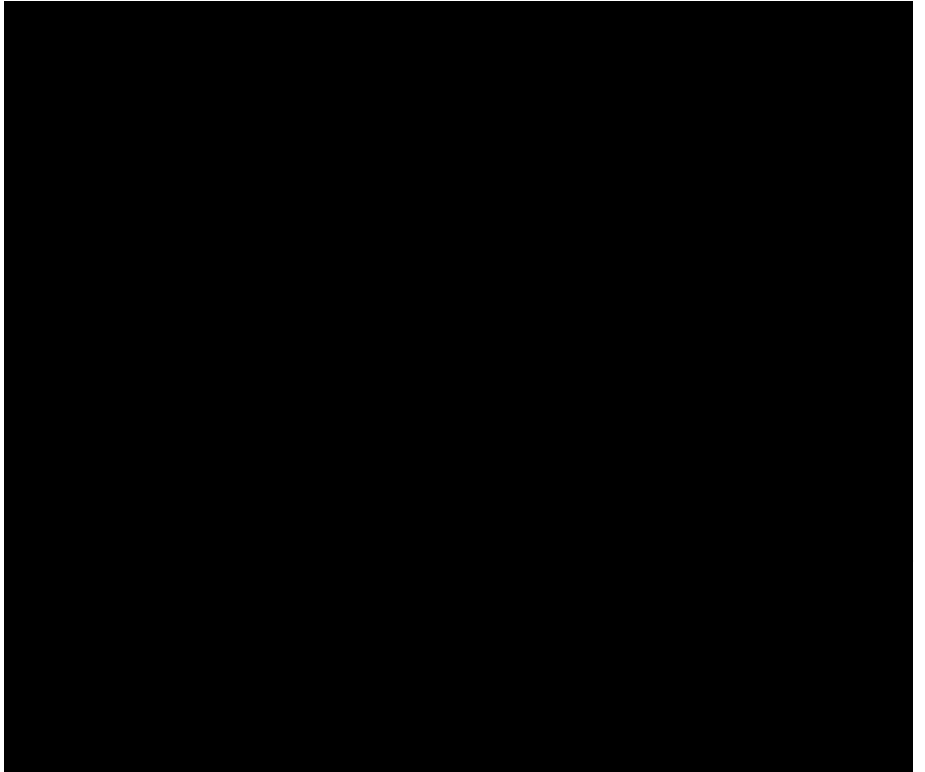
### 6.3 Other Treatments of the Calculation of Solar Efficiency 231

For negligible PRS loss, the contact resistivity beneath grid lines  $r_{c, \text{grid}}$  must be of the order of less than  $0.01 \text{ } \Omega \cdot \text{cm}^2$  (for AMI conditions and 7.5% grid coverage) whereas the large area contact at the rear of the cell can have  $r_{c, \text{rear}} < 0.2 \text{ } \Omega \cdot \text{cm}^2$ .

The contributions of  $R_p$  have been discussed in Section 5.2.5.

#### 6.3.1 Collection Function Analysis of the Light Current

In the foregoing examples the quantum efficiency  $\eta_{\text{ext}}$  was assumed to be independent of the applied bias voltage. However in many real cells, especially non-lattice-matched heterojunctions,  $\eta_{\text{ext}}$  is decreased by forward bias, resulting in reduced  $J_{sc}$  and  $V_{oc}$ . These cases are difficult to analyze because of the nonlinear equations involved and the lack of concrete information about the properties of the material in the depletion layer. Consideration of the variation of  $\eta_{\text{ext}}$  with bias as a perturbation on the ideal cell characteristics is a means of gaining perspective on the processes of photogenerated carrier transport



without resorting to the solution of a nonequilibrium transport equation in the depletion layer. This approach assumes a linear superposition of  $J_{\text{diff}}$  and  $J_L$  in the depletion layer and is therefore good only to first order. In many cases this approach simply involves including the bias- and/or wavelength-caused perturbation in each of the components and factors of the quantum efficiency expression. The result can be assembled into a factor called a collection function  $H(X, V)$  that multiplies the ideal cell  $J_L$ , giving a general expression for the J-V characteristic:

$$J = J_0 [\exp(qV/AkT) - 1] - H(\lambda, V)J_{L0} \quad (6.20)$$

where  $J_{L0}$  is the  $H = 1$  value of the light current.  $J_{L0}$  can sometimes be obtained by measurement at large reverse bias.

The general effect of an  $H < 1$  on the J-V characteristics is shown in Fig. 6.19, where the value of the light-generated current collected is reduced with respect to that generated in the absorber, especially for forward bias. As a result  $V_x$  is reduced slightly and there is a considerable reduction in  $\eta$ . The reduction in  $\eta$  is usually quite small in efficient cells. The collection function  $H$  can be measured by comparison of light and dark J-V curves or by ac methods, but the experimenter must first verify that the diode parameters  $A$  and  $J_0$  are relatively invariant with illumination, or at least account for such variations.

An example of the collection function analysis is that given by

$$J = J_0 [\exp(qV/AkT) - 1] - H(\lambda, V)J_{L0} \quad (6.20)$$

Mitchell et al. (1977) for a CdS/CdTe cell where a considerable portion of the

Fig. 6.19. Schematic J-V curves showing the effect of a collection function. Dashed curve is the dark J-V curve displaced by the large reverse bias value of JL.

useful absorption occurs in the CdTe side of the depletion layer. No appreciable useful absorption takes place in the CdS window layer, and  $J_0$  and  $A$  are almost independent of light intensity. The collection function  $H$  is a product of two factors; the first,  $g(X, V)$ , represents the bulk processes of absorption and recombination, and the second,  $h(V)$ , represents the bias dependence of interfacial recombination loss. An example of a linear formulation for the collection of photogenerated carriers from the thick, quasi-neutral region is (see Fig. 5.1 for coordinates):

$$g_1(\lambda, V) = \exp[-\alpha(\lambda)W_d(V)]/[1 + 1/\alpha(\lambda)L_n] \quad \text{for } x_p < x < \infty. \quad (6.21)$$

A second term for collection in the depletion layer of width  $W_d(V)$ , where the carriers are assumed to be swept out by the junction field without suffering recombination loss, is

$$g_2(\lambda, V) = \{1 - \exp[-\alpha(\lambda)W_d(V)]\} \quad \text{for } 0 < x < x_p \quad (6.22)$$

WAVELENGTH ( $\mu\text{m}$ )

Fig. 6.20. Measured (and smoothed) spectral response for a CdS/CdTe heterojunction prepared by vacuum evaporation of CdS onto single-crystal p-CdTe, at applied biases of zero and -1 V, reverse. Data are corrected for 13% reflection loss. A value of  $S_0 \Rightarrow 2 \times 10^{14} \text{ cm sec}^{-1}$  was



$$g_1(\lambda, V) = \exp[-\alpha(\lambda)W_d(V)]/[1 + 1/\alpha(\lambda)L_n] \quad \text{for } x_p < x < \infty. \quad (6.21)$$



$$g_2(\lambda, V) = \{1 - \exp[-\alpha(\lambda)W_d(V)]\} \quad \text{for } 0 < x < x_p, \quad (6.22)$$



deduced from these data. [From K. W. Mitchell, A. L. Fahrenbruch, and R. H. Bube, J. Appl. Phys. 48, 4365 (1977).]

where  $x = 0$  is the interface position and  $g = g_1 + g_2$ . The depletion layer width  $W_n = x_p$  is almost all in the CdTe for a heavily doped window layer and  $W_t(V) \approx [2\epsilon_s(V_d - V)/qN_A]^{1/2} \approx x_p$ .

In this case, the recombination of photogenerated carriers at centers close to the disordered interface of the CdS/CdTe heterojunction was not a function of wavelength, and Mitchell et al. (1977) made use of an approximate interfacial collection function  $h(V)$  due to Rothwarf (1976).

$$h(V) = 1/[1 + (S_i/\mu n E)], \quad (6.23)$$

where the electric field at the interface is  $E \approx 2(V_d - V)/W_d(V)$ ,  $S_i$  is the interfacial recombination velocity, and  $n$  is the local mobility. The spectral response of Mitchell's cell in Fig. 6.20 shows no appreciable variation of the ratio  $H(V=0)/H(V=1)$  over most of the wavelength range, indicating that in this range  $h(V)$  is constant with wavelength. The shape of the curves depends on wavelength and is almost independent of bias voltage in this range, so  $g = g(A)$  and  $g \propto (V_0 - V)$ . Thus this analysis argues that the observed variation in  $H$  with voltage over most of the wavelength range is due only to bias-dependent interface recombination losses occurring in regions that are thin compared to the absorption length  $1/a \approx 0.2$  /nm.

### 6.3.2 Holistic Analysis of Solar Cells

For more complex systems, a global

$$W_d(V) \approx [2\epsilon_s(V_d - V)/qN_A]^{1/2} \approx x_p.$$

$$h(V) = 1/[1 + (S_i/\mu n E)], \quad (6.23)$$

treatment of the entire solar efficiency calculation with computer-numerical solutions may be required. An example of such a system is a high-intensity cell where a high injection condition exists and the minority carrier lifetime is not constant with carrier density or position. Forward bias may influence the lifetime in the absorber quasi-neutral region and alter the J-V characteristics as well. In this case, one must return to a solution of the transport equations (perhaps simultaneous solution of the electron and hole equations with Poisson's equation) using a variable lifetime. The cell is divided into finite elements, and a relaxation solution is sought for each bias voltage in order to generate an I-V relation. Such treatments have been applied by Fossum (1976) and Spadema and Navon (1978) for concentrator cells, Dunbar and Hauser (1976a, b) for Si cells, and Hutchby and Fudurich (1976; see also Sutherland and Hauser, 1976) for graded-gap AlGaAs/GaAs structures.

#### 6.4 THE EFFECT OF TEMPERATURE AND ILLUMINATION ON CELL EFFICIENCY

The ranges of intensity and temperature encountered for space use of photovoltaic are  $0.03 < P_m < 2$  (where  $P_m$  is the solar intensity at the earth's radius) and  $-125$  to  $+140^\circ\text{C}$ , corresponding to the orbits of Jupiter and Mercury. For terrestrial concentrator systems, the intensity may exceed  $10^3$ , and the temperature is controllable to within  $5$ - $10^\circ\text{C}$  above the heat sink



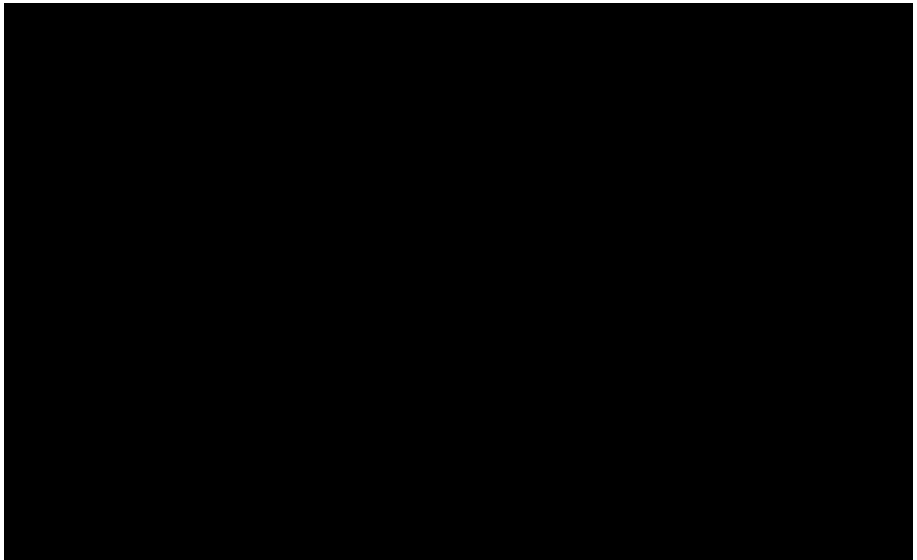
temperature (which may be held at  $T > 100^{\circ}\text{C}$  if extraction of thermal energy is desired).

#### 6.4.1 Dependence of $J_0$ and $A$ on Illumination Level

Some of the heterojunctions, MIS cells, and the  $\text{Cu}_x\text{S}/\text{CdS}$  cell in particular show a variation of the diode  $J_0$  and/or  $A$  factor with illumination level and/or wavelength. This is particularly true when trapping centers at or near the junction are not in good thermal communication with the conduction or valence bands (i.e., "slow states") and can have their occupancy, and hence charge, changed by illumination. This effect has also been observed in Si cells to a more limited extent. The change in  $J_0$  and  $A$

Fig. 6.21. Comparison of dark  $\log J$  versus  $V$  data (open circles) with  $\log JK$  versus  $V_{<^*}$  data (filled circles) for a pin junction Si cell. This cell (a NASA terrestrial reference standard) has a solar efficiency of 13.6% at AM1. Apparent  $J$ , and  $A$  values are shown.

can be due to optical absorption by states at the interface, in the bulk material near the junction, or in the insulating layer of MIS cells, any of which can produce changes in the junction profile. In the case of  $\text{Cu}_x\text{S}/\text{CdS}$ , the effect is caused by a change in ionized donor or acceptor density upon illumination, which in turn modifies the depletion layer width, the shape of the junction barrier, and, finally, the junction transport. Although the same impurity centers are responsible for



photoconductivity in homogeneous CdS:Cu (CdS doped with Cu), with similar spectral and temperature response, the junction effects are not a result of simple photoconductivity in the CuxS/CdS case (Fahrenbruch and Bube, 1974).

Differences between dark  $\log J$  versus  $V$  characteristics and a  $\log$  versus  $V^*$  plot, obtained by varying the light intensity, reveal a dependence of  $J_0$  and/or  $A$  on illumination. Data for a Si homojunction cell are shown in Fig. 6.21. However, since the illumination level varies so widely in these measurements, it is usually impossible to discriminate between changes in  $J_0$  or  $A$  or to quantify these effects. This method also cannot discriminate between changes in  $J_0$  and/or  $A$  and a bias-voltage-dependent quantum efficiency  $H(V)$ . The  $\log$  versus  $V_{oc}$  plot does remove the effect of small to moderate  $R_s$  from the characteristic however. In the extreme case of the CuxS/CdS cell,  $J_0$  and/or  $A$  change sufficiently that the light and dark  $J$  versus  $V$  curves cross.

More quantitative information about the dependence of  $J_0$  and  $A$  can sometimes be obtained by comparison of the dark  $J$  versus  $V$  curve with the  $J$  versus  $V$  curve taken at constant illumination level (by adding  $7L$  to the latter curve). The range of data for this measurement is limited to higher currents by the accuracy of the measurement of  $J_L$  however. The effect of  $H(V)$  must be either negligible or accounted for in some way as well.



## 6.4.2 Thermal Behavior

The temperature dependence of the solar efficiency can be interpreted in terms of the individual temperature dependences of  $J_{sc}$ ,  $V_{oc}$ , and  $\eta$  (e.g., Wysocki and Rappaport, 1960).

The value of  $\eta$  depends on temperature primarily through the terms involved in the minority carrier diffusion length:  $L = (nkT\tau/q)^{1/2}$ . If a cell has high quantum efficiency  $\eta_0 \gg 1$  initially, then changes of  $L$  with temperature do not substantially affect  $\eta_0/q$  [see Eq. (4.19)]; only in cells with low initial  $\eta_0$  can changes in  $L$  appreciably affect  $\eta$ . With this caveat in mind, the effects of temperature on  $L$  and  $\eta$  are discussed.

The variation of minority carrier lifetime  $\tau$  with temperature is complex, depending on the relative location of the energy levels of the recombination centers and the quasi-Fermi levels as well as the temperature dependence of the recombination cross sections of the centers themselves. As a simple example, consider a donorlike recombination center with energy level at  $E_c - \epsilon$ , and a coulomb-attractive cross section  $\sigma_0$ , that decreases with increasing temperature as  $T^{-3/2}$ . Thus,  $\tau_0 = 1 / (v_{th} \sigma_0 N_c)$  varies as  $T^{3/2}$ . Using the Shockley-Read formulation of Eq. (3.56), calculation shows that the electron lifetime  $\tau_n$ , near 300°K is approximately  $T^{3/2}$  and increases slowly with increasing temperature until  $\tau_n$  approaches the value  $\tau_0$ . For values of  $\epsilon$ ,

exceeding the strong temperature dependence of  $n$ , causes  $r$  to increase almost exponentially with  $T$ . The experimentally observed variation of  $t_{eff}$  for Si is a rather gradual increase with increasing  $T$  (approximately as  $T^{+1}$ , i when  $T$  is close to 300°K and for low injection conditions (Othmer and Chen, 1978). Mathur et al. (1981) give additional experimental results.

The dependence of the mobility on temperature is determined by the dominant scattering mechanisms. For example, if acoustic scattering is dominant, then the mobility varies with  $T^{-m}$ , where  $m = 1.5$  in the simplest case (Section 3.3). For Si, the observed variation of  $f_{jL}$  is as approximately  $T^{-*}$  for moderately doped material, and thus  $L$  varies quite slowly with temperature. In the case of GaAs, the increase in  $L$  with increasing  $T$  is somewhat stronger due to a larger variation of  $T$  with  $T$ .

The small shift of the optical absorption edge energy with temperature produces changes in  $J_{sc}$  when convoluted with the solar spectrum. These changes are relatively minor [e.g., for Si,  $(\Delta J_{sc}/79C)/\Delta T = 0.03\%/^{\circ}C$ ]. A small increase in  $J_{sc}$  with increasing temperature also results from the change of the absorption coefficient itself with temperature (Shuinka, 1970).

Experimentally,  $J_{sc}$  for most good Si cells is nearly constant, increasing slowly with temperature. An example is shown in Fig. 6.22.



The decreases in  $V^*$  and  $ff$  with increasing temperature arise mainly from changes in  $n_i$ ; the value of  $J_0$  increases exponentially with decreasing  $1/T$  causing  $V_{oc}$  to decrease almost linearly with increasing  $T$ . The variations shown by the following equations, written for one side of a homojunction with  $A = 1$ , serve to describe the general case:

$$V_{oc} = (kT/q) \ln(J_{sc}/J_0) \quad (6.24)$$

with

$$J_0 = \{D/\tau\} n_i^2 / N_A = BT^3 (D/\tau)^{1/2} \exp[-E_g/kT], \quad (6.25)$$

where the terms that are relatively temperature independent have been collected in the constant  $B$ . Then

$$V_{oc} = (E_g/q) - (kT/q) \ln[(D/\tau)^{1/2} T^3 B / J_{sc}], \quad (6.26)$$

and the logarithmic term is larger than zero and varies slowly with temperature. An example is shown in Fig. 6.22.

The temperature variation of  $V^*$  is often used to estimate the effective barrier height for experimental photovoltaic devices. For example, from Eq. (6.26) for one half of a Shockley diode, extrapolation of experimental  $V^*$ , versus  $T$  data to  $T = 0^\circ\text{K}$  should yield an intercept of the  $T = 0^\circ\text{K}$  value of  $E_g/q$ . Similarly, extrapolation of  $V_{oc}$  data for a heterojunction (e.g., with small band gap  $E_g$ ) or a Schottky diode (with barrier height  $\phi_b$ ), in which thermal activation dominates the current transport, yields approximately  $E_g/q$  or  $\phi_b$ , respectively. This is true even if the diode factor for the homojunction or heterojunction is greater than one, so long

$$V_{oc} = (kT/q) \ln(J_{sc}/J_0) \quad (6.24)$$

$$J_0 = (D/\tau)^{1/2} n_i^2 / N_A = BT^3 (D/\tau)^{1/2} \exp[-E_g/kT], \quad (6.25)$$

$$V_{oc} = (E_g/q) - (kT/q) \ln[(D/\tau)^{1/2} T^3 B / J_{sc}], \quad (6.26)$$

For Si,  $dE_f/dT = -4 \times 10^{-5} \text{ eV/}^\circ\text{C}$  and, at  $E_f = 1.1 \text{ eV}$ , the AM1.5 spectrum is such that  $dV/dE = 1.5 \times 10^{17} \text{ photons cm}^{-2} \text{ sec}^{-1} \text{ eV}^{-1}$ . Spadema and Navon (1978) discuss the influence of temperature variation on optical absorption.

#### TEMPERATURE ( $^\circ\text{C}$ )

Fig. 6.22. Photovoltaic parameters for an experimental, 4-cm<sup>2</sup> Si cell versus temperature (for P,  $\sim 140 \text{ mW cm}^{-2}$ ). The  $V_{oc}$  curve has been extrapolated to  $T = 0^\circ\text{K}$  [Data from R. K. Yasui and L. W. Schmidt, Proc. 8th IEEE Photovoltaic Specialists Conf. (1970), p. 110.]

as tunneling processes are not involved. The extrapolation to  $0^\circ\text{K}$  does not yield in any case. For most simple transport models that do not involve tunneling, the (FK) extrapolation from data in the  $77^\circ\text{K}$  to  $300^\circ\text{K}$  range overestimates  $E_f/q$  or  $I_{sc}$  by at least 5%, because of the small temperature variation of the logarithmic term in Eq. (6.26).

In general,  $ff$  decreases quite strongly with temperature as shown in Figs. 6.22 and 6.23. The variation can be calculated using Eqs. (6.8) and (6.10), but the mathematics are too involved to be particularly enlightening.

For Si-based homojunction cells, the solar efficiency  $\eta$  reaches a maximum at  $-150^\circ$  to  $-100^\circ\text{C}$ ; near  $25^\circ\text{C}$ , the efficiency decreases at the rate of  $\Delta\eta/\Delta T = -0.05$  percentage points per Celsius degree, as shown in Fig. (6.22). A good comparison of

the variation of theoretical and experimental photovoltaic parameters with temperature for Si cells is given by Arora and Mathur (1981).

Fig. 6.23. Photovoltaic parameters for an AlGaAs/GaAs solar cell versus temperature at AMO. At 25°C,  $\eta = 16.4\%$ . [Data from "GaAs Concentrator Photovoltaic Power System Feasibility Investigation," AFAPL-TR-76-C-2142. Hughes Aircraft Co., Torrance, California. 1977. Figure redrawn from C. Stuerke, Proc. 13th IEEE Photovoltaic Specialists Conf. (1978), p. 551, © 1978 IEEE.]

For GaAs-based cells, the peak in  $\eta$  occurs at a higher temperature, -100° to -50°C, because of the relatively stronger increase in  $L$  with temperature commonly seen in GaAs. The rate of decrease of  $\eta$ , in percentage points, is  $\Delta\eta/\Delta T = -0.033$  per Celsius degree near 25°C as shown in Fig. 6.23.

The temperature dependences of other devices where the current transport is mainly by thermal injection, such as heterojunctions and Schottky barrier cells, are qualitatively similar to the preceding example (Fischer-Colbrie et al., 1976). For heterojunctions,  $\eta$  at elevated temperatures generally increases quite strongly with increasing band-gap energy of the smaller band-gap component as suggested by Fig. 6.5. Thus higher band gaps are more suited to



concentrator and other high temperature systems.

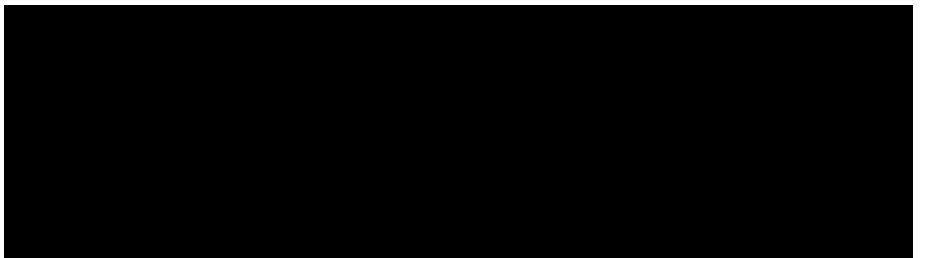
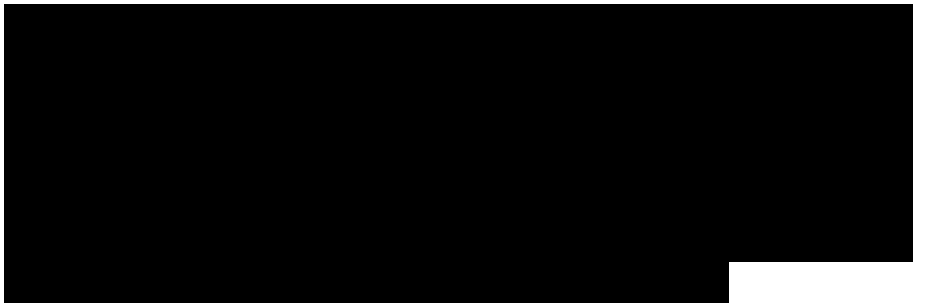
In cases where the current transport is controlled at least partially by tunneling, such as in Cu<sup>s</sup>/CdS and MIS cells, the  $V_{oc}$  and  $ff$  might be expected to be somewhat more independent of temperature. The thermal variation of the photovoltaic parameters of MIS cells appears to be relatively unexplored at this time.

Low-temperature operation poses special problems:  $L$ , and hence  $J_x$ , can decrease considerably if the mobility is dominated by charged impurity scattering. Contacts may become nonohmic at low temperatures, causing large losses in  $ff$ . The latter problem in Si cells has been largely overcome by the technology of Al-diffused p<sup>\*</sup> back surface layers.

#### 6.4.3 High-Intensity Effects

The variation of solar efficiency with illumination intensity is best treated holistically by computer analysis because of the complexity of the equations involved. This has been done by Spadema and Navon (1978) for example. However, it is physically insightful to treat the variation of  $\eta$  with intensity by separate consideration of  $J_x$ ,  $V_{oc}$ , and  $ff$ , as in the previous section. It is found that series resistance effects on  $ff$  are usually more crucial than the rise in cell temperature due to high illumination levels.

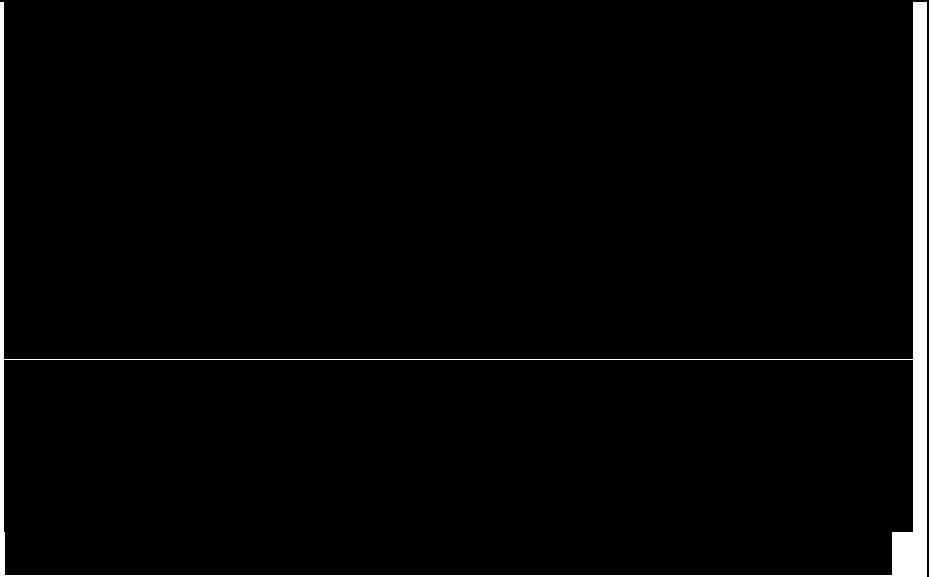
The light-generated current ( $J_L = J_x$ ) is proportional to photon flux  $T$  as long as the minority carrier lifetime in the absorber is constant. At higher photon fluxes however, increased carrier traffic begins to



saturate the recombination centers, increasing the lifetime and thus producing an increase in quantum efficiency (Vasil'ev et al., 1975). For the example of donorlike recombination centers with energy level  $\epsilon_c = E_t$  in a p-type absorber, the lifetime is approximately constant ( $\tau_{eff} \approx \tau_{r0}$ ) with increasing photogenerated carrier density until  $n_p$  approaches  $(N_{D0} / \tau_{r0})$ , as indicated by Eqs. (3.45) and (3.56). At electron densities exceeding this, the lifetime increases substantially, as shown in Fig. 3.15, producing a superlinear relation between  $J_L$  and  $T$  for cells with initially low  $\tau_{r0}$ . For cells with initially high  $\tau_{r0}$ , the change in  $\tau_{r0}$  with illumination level is small, e.g., because of the form of Eq. (4.19) and the superlinearity is negligible. Ho et al. (1977) and Ho and Mathias (1978) observed such a superlinearity of the  $J_L$  versus  $F$  relation for Si EFG ribbon cells. Their data correlated well with separate measurements showing an increase of the minority carrier diffusion length with increasing photon flux.

The open-circuit voltage increases with intensity as  $\ln[yL(D/70)]$  until, at high injection levels, more complex effects come into play. These effects include the voltage drop across the depletion layer at the junction, which becomes appreciable at high  $V_{oc}$ , and a change from  $A = 1$  transport to high injection,  $A = 2$  transport as outlined in Section 5.2.5.

An interesting example of high-intensity effects in a p-i-n junction is



t The thermal and electronic aspects of high-intensity operation are discussed in Chapter

} For a coulomb attractive, donorlike recombination center  $T^*$ ,  $=*$  KK'T.O, for example.

"Fig. 6.24. Current-voltage characteristics for a Si p/i/n junction solar cell under high illumination. [Redrawn from R. Swanson, "Silicon Photovoltaic Cells in TPV Conversion," EPRI ER-633, Proj. 790-1, Interim Rep. (1978).J

shown in Fig. 6.24, where the lifetime in the front part of the absorber layer is thought to increase when the density of minority carriers there is increased by forward-bias injection. Thus, at forward bias, JL actually appears to increase with respect to its zero bias value.t

For zero  $R_s$ , the fill factor  $ff$  increases slowly with intensity, as shown by Fig. 6.11. The effect of nonzero  $R_t$  on  $ff$  becomes crucial at high intensities. In order for the  $R_s$  loss to be negligible we must have  $R_s < V_{oc} S \rho / J^*$ , where % is allowed fractional PR, power loss given by Eq.(6.11) . For AMI conditions a rule-of-thumb value is  $0.5 \text{ Cl cm}^2$  so, at higher intensities,  $R_h s [0.5/C]$   $\text{il cm}^2$ . For a  $C = 1000$  system, the necessary  $R_s < 0.0005 \text{ H cm}^2$  is difficult to achieve and requires closely spaced grid lines, low contact resistivities, and/or special grid geometries.t The variation of  $ff$  with concentration ratio for several values of  $R_s$  is also shown in Fig. 6.11, assuming no thermal effects.



Given good heat sinking,  $T_J$  increases almost logarithmically with increasing intensity until high injection and series resistance effects cause

t R. Swanson, personal communication, Dcp. Electr. Eng., Stanford Univ., Stanford, California (1979).

t Such special geometries include, for example, the stacked vertical multijunction cell. Section 7.6.1; and the V-groove cell. Section 12.2.3.

Fig. 6.2S. Power loss chart for Si cell operating at AM1.5 (Fig. 6.3). Percentage of total input power  $P$ , lost to each of the loss mechanisms is noted. The  $R_t$  loss is included in  $J_t$ . Values of  $J_t = 5 \times 10^{-11} \text{ A cm}^{-2}$  and  $A = 1$  for the diode are assumed.

it to saturate or even decrease with increasing  $C$  (see Fig. 8.11, for example).

### 6.5 LOSS ANALYSIS

Energy loss analysis is a powerful tool for cell optimization; each loss mechanism can be put into proper perspective and attacked separately to optimize the efficiency of the device. Such an analysis, similar to that done by Wolf (1971), is shown in Fig. 6.25. The major contributions are listed here:

- (1)  $h\nu > E_g$  thermalization of hot carriers to near the band edge,
- (2)  $h\nu < E_g$  low-energy photons pass through the cell without pair generation,
- (3)  $T_J Q$  collection efficiency for photogenerated carriers,

determined by diode parameters, principally thermalization of carriers over potential barrier, loss in the diode forward-biased to  $V_m$ , PR losses in series and parallel resistance (usually included in  $ff$ ), reflection of photons at light-incident surfaces, grid coverage,

- (4)  $qV_M < \epsilon, \lambda_i$
- (5) Fill factor ( $ff$ )
- (6)  $R_s, R_p$
- (7) Reflection loss
- (8) Area factor
- (9) Spurious absorption

absorption in antireflection coating, at defects, etc.

Of these, the first two are unavoidable except by the use of graded gap structures, spectral splitting cells, or spectral conversion (see Chapter 12). Item 3,  $qV_M < \epsilon$ , is a consequence of both the thermodynamic efficiency of the diode for separation of charge and of the diode parameters themselves. Items 3 through 9 remain available for optimization.

Trong những yếu tố này, hai yếu tố đầu tiên không thể nào tránh được nếu không dùng các cấu trúc có độ rộng vùng cấm phân cấp, các loại pin phân chia phổ, hoặc chuyển đổi phổ (xem Chương 12). Yếu tố thứ 4,  $qV_{oc} < E_g$  là hệ quả của cả hiệu suất động lực học của diode trong quá trình phân ly điện tích và chính các tham số diode. Các yếu tố từ 3 đến 9 có thể tối ưu hóa được.